FEMS Microbiology Ecology, 92, 2016, fiw171

doi: 10.1093/femsec/fiw171
Advance Access Publication Date: 10 August 2016
Research Article

RESEARCH ARTICLE

Composition of diatom communities and their contribution to plankton biomass in the naturally iron-fertilized region of Kerguelen in the Southern Ocean

Marine Lasbleiz[1,*], Karine Leblanc[1], Leanne K. Armand[2], Urania Christaki[3], Clément Georges[3], Ingrid Obernosterer[4] and Bernard Quéguiner[1]

[1]Aix-Marseille Université, Université de Toulon, CNRS/INSU, IRD, MIO, UM 110, 13288, Marseille, Cedex 09, France, [2]Department of Biological Sciences, Macquarie University, North Ryde, New South Wales, 2109, Australia, [3]INSU-CNRS, UMR8187 LOG, Laboratoire d'Océanologie et des Géosciences, Université du Littoral Côte d'Opale, ULCO, 32 avenue Foch, 62930 Wimereux, France and [4]CNRS, Sorbonne Universités, UPMC Univ Paris 06, Laboratoire d'Océanographie Microbienne (LOMIC), Observatoire Océanologique, F-66650 Banyuls/mer, France

*Corresponding author: Mediterranean Institute of Oceanography, Aix-Marseille Université, Bâtiment OCEANOMED, campus de Luminy, case 901, F-13288 Marseille, Cedex 09, France. Tel: +33-486-09-05-72; E-mail: Marine.lasbleiz@gmail.com

One sentence summary: The phenology of the naturally iron-induced phytoplankton blooms east of the Kerguelen Islands was investigated by documenting the spatial and temporal variation of phytoplankton community structure concurrently with biogeochemical observations.

Editor: Gary King

ABSTRACT

In the naturally iron-fertilized surface waters of the northern Kerguelen Plateau region, the early spring diatom community composition and contribution to plankton carbon biomass were investigated and compared with the high nutrient, low chlorophyll (HNLC) surrounding waters. The large iron-induced blooms were dominated by small diatom species belonging to the genera *Chaetoceros* (*Hyalochaete*) and *Thalassiosira*, which rapidly responded to the onset of favorable light-conditions in the meander of the Polar Front. In comparison, the iron-limited HNLC area was typically characterized by autotrophic nanoeukaryote-dominated communities and by larger and more heavily silicified diatom species (e.g. *Fragilariopsis* spp.). Our results support the hypothesis that diatoms are valuable vectors of carbon export to depth in naturally iron-fertilized systems of the Southern Ocean. Furthermore, our results corroborate observations of the exported diatom assemblage from a sediment trap deployed in the iron-fertilized area, whereby the dominant *Chaetoceros* (*Hyalochaete*) cells were less efficiently exported than the less abundant, yet heavily silicified, cells of *Thalassionema nitzschioides* and *Fragilariopsis kerguelensis*. Our observations emphasize the strong influence of species-specific diatom cell properties combined with trophic interactions on matter export efficiency, and illustrate the tight link between the specific composition of phytoplankton communities and the biogeochemical properties characterizing the study area.

Keywords: diatoms; carbon biomass; plankton community structure; natural iron fertilization; Southern Ocean

Received: 2 May 2016; **Accepted:** 5 August 2016

INTRODUCTION

Several decades of careful oceanographic research has allowed the identification of key biogeochemical processes influencing control on the biological carbon (C) pump (e.g. Legendre and Le Fèvre 1989; Nelson *et al.* 2002; Smetacek *et al.* 2012). The impact produced by such processes on C export to the deep ocean remains, however, insufficiently documented as a result of the limited number of particle flux studies. In this context, understanding the complex interactions between phytoplankton communities and oceanic biogeochemical cycles has been specifically highlighted as requiring more focused research (Boyd 2013).

Diatoms are silicified phytoplankton, and are recognized as one of the main vectors of C export in the Southern Ocean (e.g. Buesseler *et al.* 2005; Romero and Armand 2010; Rigual-Hernández *et al.* 2015a). Recent studies have begun to focus on the wide variation in diatom morphology, elemental composition, community structure and aggregate formation as additional factors in understanding C export efficiency (Assmy *et al.* 2013; Quéguiner 2013; Sackett *et al.* 2014). These factors indeed influence the sinking rates of particles, their transfer to higher trophic levels and their remineralization in the water column (e.g. Armstrong *et al.* 2009; Salter *et al.* 2012; Rigual-Hernández *et al.* 2015b).

Diatoms are particularly responsive to the addition of iron in regions of the Southern Ocean characterized by high nutrient, low chlorophyll (HNLC) regimes (e.g. de Baar *et al.* 2005). Extensive blooms of diatoms are recurrently observed east of Kerguelen Island due to the natural iron fertilization of the surface waters, located in the wake of the Antarctic Circumpolar Current (Blain *et al.* 2007; Armand *et al.* 2008; Lasbleiz *et al.* 2014). Therefore, the Kerguelen region represents a unique natural laboratory to study the impact of iron on the functioning of plankton communities and associated biogeochemical cycles. The first Kerguelen Ocean and Plateau Study (KEOPS) cruise (KEOPS 1) was conducted in this region in late summer (January–February 2005) and demonstrated enhanced C export efficiency of the naturally iron-fertilized system situated within a typical HNLC region (Blain *et al.* 2007). Plankton community composition was clearly different between the iron-fertilized and the HNLC areas (Armand *et al.* 2008; Carlotti *et al.* 2008; Christaki *et al.* 2008; West *et al.* 2008). These community-scale observations, across and within the studied locations, confirmed the strong link between plankton community composition and their related biogeochemical cycles.

The present study is focused on the early bloom stages of the naturally iron-fertilized Kerguelen Plateau system (October–November 2011, KEOPS 2), and therefore is placed in the context of the previous study that examined the bloom pinnacle and decline (KEOPS 1; Mosseri *et al.* 2008). During the KEOPS 2 program, the biogeochemical drivers underpinning plankton community structure (from viruses to mesozooplankton) and succession, and the consequent impact on C export efficiency were investigated from many angles (e.g. Christaki *et al.* 2014; Carlotti *et al.* 2015; Planchon *et al.* 2015; Landa *et al.* 2016). In the present paper, surface diatom community composition and contribution to plankton community C biomass were considered by addressing the spatial differences between contrasted regions in terms of iron availability and mesoscale activity. Complementary net-haul and conductivity–temperature–depth (CTD) rosette samplings were conducted across the surveyed region to get the most realistic vertical picture of diatom community composition at the highest possible taxonomic level. The objectives were to (i) understand the phenology of the eastern Kerguelen blooms by comparing the spatial and temporal variation of phytoplankton community structure with concurrent biogeochemical observations, (ii) explore the island mass effect (i.e. iron availability, proximity of the coast) on diatom community composition by comparing observations in an HNLC off-plateau area, and (iii) discuss the potential impact of surface phytoplankton community structure on C export.

MATERIALS AND METHODS

Study area

The KEOPS 2 cruise was conducted in the south Indian Ocean sector of the Southern Ocean, principally to the east of Kerguelen Plateau (KP), aboard the French *R/V Marion Dufresne II* in austral spring (10 October–20 November 2011). The KP acts as a natural barrier diverting both the trajectory of the Antarctic Circumpolar Current (ACC) and the trajectory of the Polar Front (PF) (Park *et al.* 2008a; Fig. 1). Interactions between the plateau and hydrodynamic features result in natural iron inputs to surface waters to the east of the KP, which sustain large annual blooms contrasting with the HNLC surrounding waters of the Southern Ocean (Blain *et al.* 2007; Park *et al.* 2014a; Quéroué *et al.* 2015).

Composite satellite images (produced by F. Nencioli, KEOPS2 website: http://keops2.obs-vlfr.fr/) showed that the 2011 Kerguelen bloom developed rapidly from mid-October with a large spatial heterogeneity leading to a mosaic of biogeochemical environments reflected in variations in surface water productivity (Closset *et al.* 2014; Cavagna *et al.* 2015) and particulate matter (Lasbleiz *et al.* 2014).

In this study, a total of eight stations were investigated (Fig. 1): seven stations representing iron fertilized bloom-affected regions to the northeast (E and F-L stations) and southeast (KEOPS 1 repeat station A3-2), and one station representing surrounding HNLC conditions off the plateau (R-2). The latter station was characterized by low biomass and primary production (Table 1) induced by iron limitation (Quéroué *et al.* 2015). Conversely, the stations situated in the eastern bloom within the Polar Front zone (F-L), the southeastern KP bloom (A3-2) and the eastern flank of the Kerguelen Islands (E-4W) were characterized by high particulate matter concentrations (chlorophyll *a*, biogenic silica), and high primary production and biogenic silica production (Table 1). The onset of the bloom was offset locally inside the meander of the PF in the northeastern KP region, as shown by intermediate biomass levels, and moderate primary and biogenic silica productions (Table 1). This area, corresponding to a quasi-stagnant feature (Park *et al.* 2014b), was sampled temporally (E-1, E-3, E-4E and E-5) as part of a pseudo-Lagrangian survey. A drifter-derived velocity field (Park *et al.* 2014b) suggested, however, that E-4E corresponds to a distinct physical feature from the other three E stations. Therefore, in this study, E-4E was excluded from the time-series (E-1, E-3, E-5).

Diatom sampling and enumeration

For each station, samples were collected from both vertical net hauls and CTD rosette casts providing, respectively, qualitative and quantitative information on the diatom community composition.

Net haul sampling

A 35 μm mesh phytoplankton net was deployed to sample the top 100 m of surface waters. On board, 1 mL aliquot was placed

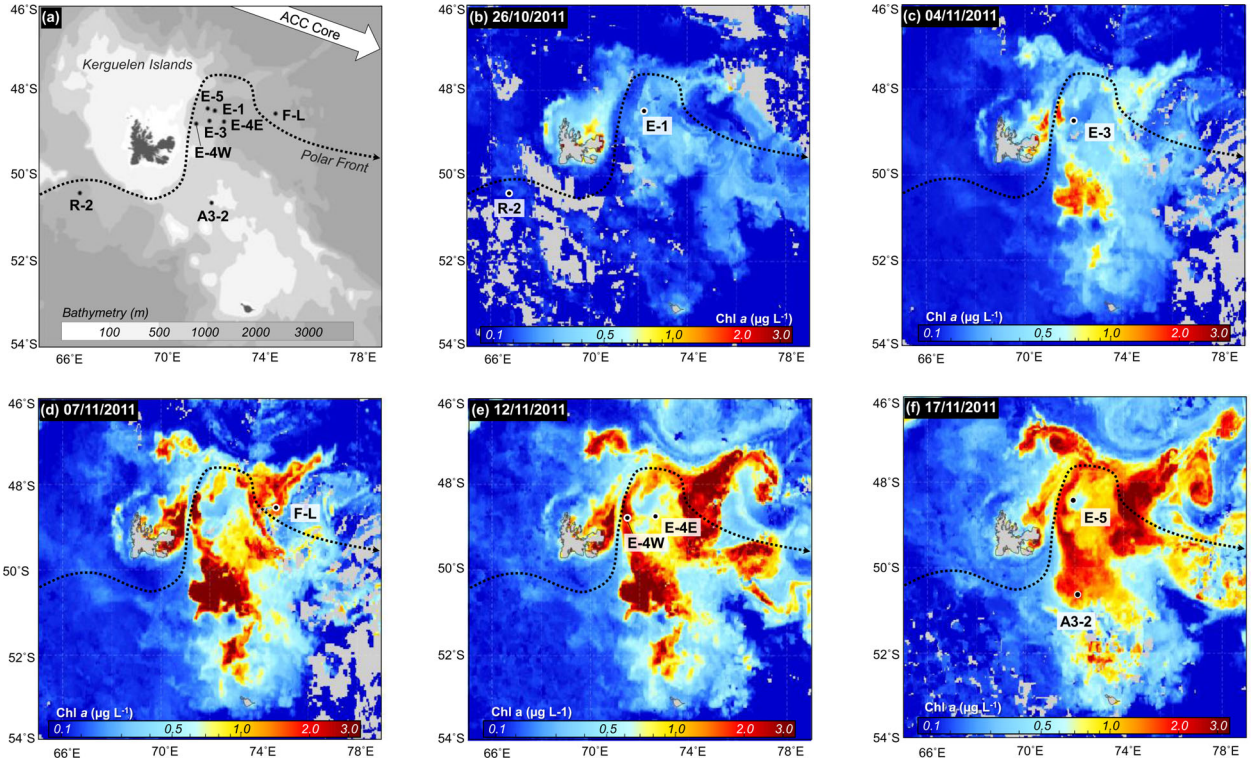

Figure 1. Location of the eight sampling stations (**a**) and MODIS-Aqua satellite (CLS-CNES) images of surface chlorophyll *a* concentration (Chl *a*) representative of phytoplankton bloom stages at the sampling time of each station (**b–f**). R-2 is the HNLC reference station. F-L is located in the eastern bloom within the Polar Front zone. The stations A3-2 and E-4W are respectively the reference southeastern Kerguelen Plateau bloom and the reference eastern flank of the Kerguelen Island. The stations E-1, E-3, and E-5 correspond to a time series of the recirculation system in the meander of the Polar Front. E-4E is located further east compared with the three latter stations and was associated to a distinct physical feature (Park *et al.* 2014b). The dotted line represents the approximate location of the southern branch of the Polar Front and the white arrow corresponds to the Antarctic Circumpolar Current core (ACC Core) (from Park *et al.* 2014b).

in a Sedgwick–Rafter 1 mm × 1 mm gridded cell and observed under a Nikon TS100 inverted microscope. Qualitative assessment of phytoplankton community composition was made using four abundance categories: (i) dominant, when a given species was observed in all fields of view; (ii) common, when a species was observed in most fields of view (~50–80%); (iii) minor, when a species was observed less than 15 times in a sample; and (iv) rare, when a species was observed once or twice in a sample.

CTD rosette cast sampling

Seawater samples were collected from a 12 L bottle CTD rosette equipped with a Seabird SBE 911-plus CTD unit. Samples were taken at four to six depths relative to varying photosynthetically active radiation (PAR; 75–0%; Table 1). Aliquots of 250 mL were preserved with 0.8 mL acidified Lugol's solution in amber glass bottles. Bottles were then stored in the dark at 4°C until analysis.

Diatom counts were made following the Utermöhl method (Hasle 1978). For the HNLC reference station (R-2) with low chlorophyll concentrations (Lasbleiz *et al.* 2014), a 100 mL seawater sample was settled for 48 h in a settling chamber, whereas for the other stations presenting higher cell abundances only 10–25 mL samples were settled for 24 h. After settling, samples were analyzed with a Nikon Eclipse TE2000-E inverted microscope equipped with phase contrast, at ×100, ×200 or ×400 magnification. Each complete diatom cell was identified to the lowest taxonomic level using taxonomic concepts detailed in Hasle and Syvertsen (1997) while taxonomic listings (Supplementary Table S1) follow accepted names listed in the *World Register of Marine Species* (WoRMS: http://www.marinespecies.org/). Several groupings at the genus level were made due to the difficulty of separating some species at ×400 magnification. All small *Chaetoceros* (*Hyalochaete*) species were grouped together although the dominant contributors were *Chaetoceros debilis* and *Chaetoceros curvisetus*. *Fragilariopsis rhombica* and *Fragilariopsis separanda* species could not be differentiated under inverted microscopy and were grouped under the term '*Fragilariopsis rhombica/separanda*'. For the same reasons, the *Tropidoneis* group encompasses *Membraneis* and *Plagiotropsis* species as well as *Haslea trompii*. *Thalassionema nitzschioides* was represented by three varieties: mainly *T. nitzschioides* var. *nitzschioides*, accompanied with *T. nitzschioides* var. *parva* and *T. nitzschioides* var. *lanceolata*. The term 'centric spp. (<25 μm)' corresponds to an assemblage of small centric diatoms composed principally of several *Thalassiosira* species and *Actinocyclus* spp. Live cells and empty frustules were identified from all preserved CTD samples. Frustules with no chloroplasts visible to the eye during observation were considered as empty. This category does not include broken cells and fragments, neither of which were tallied.

Specific diatom C biomass was assessed following the methodology of Cornet-Barthaux, Armand and Quéguiner (2007). Cell dimensions were determined from at least 10 representative images of each species from all samples using NisElement AR 2.30 software (measurement precision <1.0 μm). When not measurable due to the cell's position on the slide (e.g. the transapical axis of *Fragilariopsis kerguelensis* or the pervalvar axis of numerous centrics), the missing dimensions were calculated alternatively from the visible to hidden dimensions ratio

Table 1. Depth list of discrete water samples within the water column taken from CTD casts with their corresponding light levels expressed in terms of the percentage photosynthetically active radiation (PAR) as compared with the surface. Each station is associated with the corresponding mixed layer depth (MLD) and integrated biogeochemical properties reflecting phytoplankton productivity within the euphotic layer (i.e. layer from the surface to the depth to which 1% of surface PAR remains). Chl *a*, chlorophyll *a*; BSi, biogenic silica; GCP; gross community production; ρSi, the silica production rates.

Station	PAR (%)	Depth (m)	MLD (m)	Chl *a*[a] (mg m^{-2})	BSi[a] (mmol m^{-2})	ρSi[b] (mmol m^{-2} d^{-1})	GCP[c] (mmol m^{-2} d^{-1})
	75	2					
	25	12					
A3-2	1	38	123	83	174	48	572
	0.01	77					
	0	150					
	75	2					
E-4W	25	9	64	56	142	32	549
	1	40					
	0.01	61					
	75	2					
F-L	25	9	47	127	98	28	647
	1	35					
	0.01	57					
	75	6					
R-2	25	28	123	30	33	3	107
	1	100					
	0.3	116					
	75	4					
E-1	25	19	70	61	96	17	166
	1	64					
	0.3	81					
	75	4					
E-3	25	21	35	42	84	11	118
	1	70					
	0.01	137					
	75	3					
E-5	25	16	92	63	160	27	315
	1	55					
	0.01	108					
	75	2					
E-4E	25	10	80	56	104	21	205
	1	50					
	0.01	100					

Data from [a]Lasbleiz *et al.* (2014); [b]Closset *et al.* (2014); [c]Cavagna *et al.* (2015).

deduced from the shape of the cell (Olenina *et al.* 2006; Leblanc *et al.* 2012) When possible the ratio was also estimated from other comparable samples in which the missing dimension was occasionally measurable.

Cellular biovolume was estimated from the mean of linear dimensions using the appropriate geometric formulae reflecting the cell shape (Hillebrand *et al.* 1999; Sun and Liu 2003; Leblanc *et al.* 2012). The C content of diatoms was calculated from cellular biovolume according to the corrected equation of Eppley (Smayda 1978) as applied in Cornet-Barthaux, Armand and Quéguiner (2007).

Sampling and enumeration of plankton organisms other than diatoms

Seawater samples were collected at a minimum of 10 depths from the surface to 900 m at each station by CTD rosette to assess the C biomass contribution of major functional plankton groups other than diatoms from pico- to micro-sized organisms. The term 'functional plankton group' refers to conceptual groupings of plankton species with common biogeochemical and ecological attributes.

The abundance of heterotrophic bacteria (*sensus stricto Bacteria* and *Archaea*), heterotrophic nanoflagellates (HNF), pico- and nanophytoplankton (including *Synechococcus*, nano- and picoeukaryotes) was determined using a FACSCalibur flow cytometer (Marie *et al.* 1999; Christaki *et al.* 2011). For heterotrophic bacteria, the biomass conversion factors used were 12.4 fg C $cell^{-1}$ (Fukuda *et al.* 1998). For HNF, in order to establish the size of cells of the three cytometric populations identified during this study, cells from each population were sorted with a FACSAria cell sorter (BD Biosciences). The sorted cells (1000 to 3000 cells per sample) were collected on Nucleopore filters (0.2 μm pore size, 25 mm diameter), and examined

using a Zeiss AX10 microscope at ×1000 magnification. The mean biovolume of each cytometric population was calculated based on the linear dimensions of the cells and the mean C biomass (3.26 pg C cell^{-1}) was estimated from a conversion factor of 183 fg C μm^{-3} (Caron *et al.* 1995). For *Synechococcus*, pico- and nano-phytoplankton, conversion factors of the identified groups were established during KEOPS 1 mission according to Veldhuis and Kraay (2000) with the application of fractionated filtration steps (10, 8, 5, 3, 2, 1 and 0.6 μm). C biomasses were calculated using the empirical relationship between biovolume and cell C content (Eq. 1) of Verity *et al.* (1992):

$$0.433 \times V^{0.86} \quad (1)$$

where V is biovolume in μm^3 and cell C content is expressed in pg C cell^{-1}.

This resulted in 0.34, 0.86 and 3.81 pg C cell^{-1} for *Synechococcus*, picoeukaryotes and nanophytoplankton (<10 μm), respectively. These values are within the range of biomasses reported in a recent study in the Sargasso Sea (0.337 and 3.02–3.34 for *Synechococcus* and eukaryotic algae, respectively; Casey *et al.* 2013).

Ciliates and dinoflagellates were counted in 500 mL samples fixed in acid Lugol's solution and were identified based on their morphology at the lowest possible taxonomic level (Christaki *et al.* 2015). Ciliates and dinoflagellates were further divided into six size groups (<20, 20–40, 40–60, 60–80, 80–100 and >100 μm). Linear dimensions were measured at ×400 magnification using an image analyzer with a camera mounted on the microscope (Nikon Eclipse TE2000-S). Cell biovolume was calculated assuming the nearest geometrical shape. For these two taxa, a minimum of 10 cells (for rare species) and a maximum of 300 cells (for the most abundant species) were measured. Biovolume was then converted to C biomass based on a C:biovolume factor of 0.19 pg C μm^{-3} (Putt and Stoecker 1989) for ciliates and from the following equation (Eq. 2) for heterotrophic dinoflagellates (Menden-Deuer and Lessard 2000):

$$0.216 \times V^{0.939} \quad (2)$$

where V is biovolume in μm^3 and cell C content is expressed in pg C cell^{-1}.

Copepod *nauplii*, acantharians, foraminifera and radiolarians were counted in the same samples prepared for diatom counts in order to determine their approximate contribution to the total C biomass as compared with diatoms. We acknowledge that the sample volumes used were too small to obtain an accurate estimate of their respective abundances. Therefore, they were not included in the estimate of the total C biomass. We recommend for future studies sampling volumes and preservation techniques attuned to the appropriate estimation of these four plankton groups from the water column.

Surface water partitioning

For the purposes of comparing community carbon structure across the study stations, C biomass calculations for each plankton functional group were integrated across two distinct layers of the water column, following Buesseler and Boyd's (2009) approach. The first layer corresponds to the euphotic layer: limited by the euphotic depth (Ze), traditionally defined as the depth to which 1% of surface PAR remains. The second, subeuphotic layer underlies the euphotic layer and extends 100 m below the Ze.

RESULTS

Diatom cell abundance and biomass vertical profiles

The vertical profiles of diatom abundance demonstrating the contribution of live cells, empty frustules and C biomass estimates obtained from CTD rosette sampling are presented in Fig. 2 (detailed results are provided in Supplementary Table S2). Live cell abundances and C biomass estimates typically decreased with light attenuation through the water column, with the exception of the profiles recovered from stations R-2 and E-1. The lowest live cell abundance ($1.5 \pm 0.2 \times 10^4$ cells L^{-1}) and C biomass (3.0 ± 0.3 μg C L^{-1}) were encountered at the HNLC reference station, R-2 (Fig. 2d). These minimum values contrast starkly with the mixed-layer maximum live cell abundances, ranging from 128×10^4 to 293×10^4 cells L^{-1}, and the highest C biomasses varying between 69.3 and 274 μg C L^{-1}, derived from the highly productive stations A3-2, E-4W and F-L (Fig. 2a–c). In the PF meander stations (Fig. 2e–h), low live cell abundances and C biomasses were recorded during the two first visits (E-1 and E-3, $5.9 \pm 2.2 \times 10^4$ cells L^{-1}, 20.0 ± 5.5 μg C L^{-1}). At E-5, estimated live cell abundances and C biomass increased to $14.0 \pm 8.7 \times 10^4$ cells L^{-1} and 33.3 ± 15.4 μg C L^{-1}. Compared with the three PF meander stations E-1, E-3 and E-5, the station E-4E located further east had higher live cell abundances and C biomass ($31.8 \pm 15.0 \times 10^4$ cells L^{-1} and 40.2 ± 20.1 μg C L^{-1}).

The proportion of empty frustules increased with depth at all stations, varying on average from $6 \pm 7\%$ in the surface (75% PAR) to $24 \pm 13\%$ below the Ze. Within the euphotic layer, the lowest percentages of empty frustules (mean $3 \pm 2\%$) were observed at the high productivity stations (A3-2, E-4W and F-L) and E-4E, whilst the highest percentages (mean $20 \pm 7\%$) were found at stations R-2, E-1, E-3 and E-5 (Fig. 2; Supplementary Table S2).

Diatom community composition

Comparison of CTD rosette vs net haul samples

The comparison between CTD rosette and net haul results (Fig. 3) illustrates how the two sampling techniques complement the vertical picture of the diatom community structure. Net haul sampling highlighted the presence of large diatoms (e.g. *Corethron pennatum*, *Dactyliosolen antarctica*, *Fragilariopsis kerguelensis* and *Rhizosolenia* spp.), which were rare in CTD rosette samples. As a relevant example, the large diatom *C. pennatum* dominated the diatom assemblages in net haul samples at R-2, E-1 and E-5, but only represented less than 1% at R-2 and 5% at E-1 and E-5 of the diatom cell abundance over the water column when enumerated from CTD rosette samples. Conversely, CTD rosette sampling allowed the capture of small diatoms (e.g. centric spp. (<25 μm), *Thalassionema nitzschioides*), that were not retained by the 35 μm-mesh phytoplankton net. This difference was more pronounced at the station F-L where the small centrics (*Thalassiosira*-like), mainly present in the form of single cells rather than chain colonies as observed everywhere else over the KP region, were absent from net haul samples while they dominated cell abundances in Niskin bottles. The analysis of CTD rosette and net haul results also provided evidence that the diatom assemblages sampled from Niskin bottles were dominated (i.e. when a given species contributed to >10% of the diatom cell abundance) by fewer species/genera than were observed in the concentrated net haul samples. Common or minor species in net haul samples usually represented <1% of the total diatom cell abundance in Niskin bottles. All these observations were strong arguments for combining net haul and CTD rosette results to better meet the objectives of this study. As CTD rosette

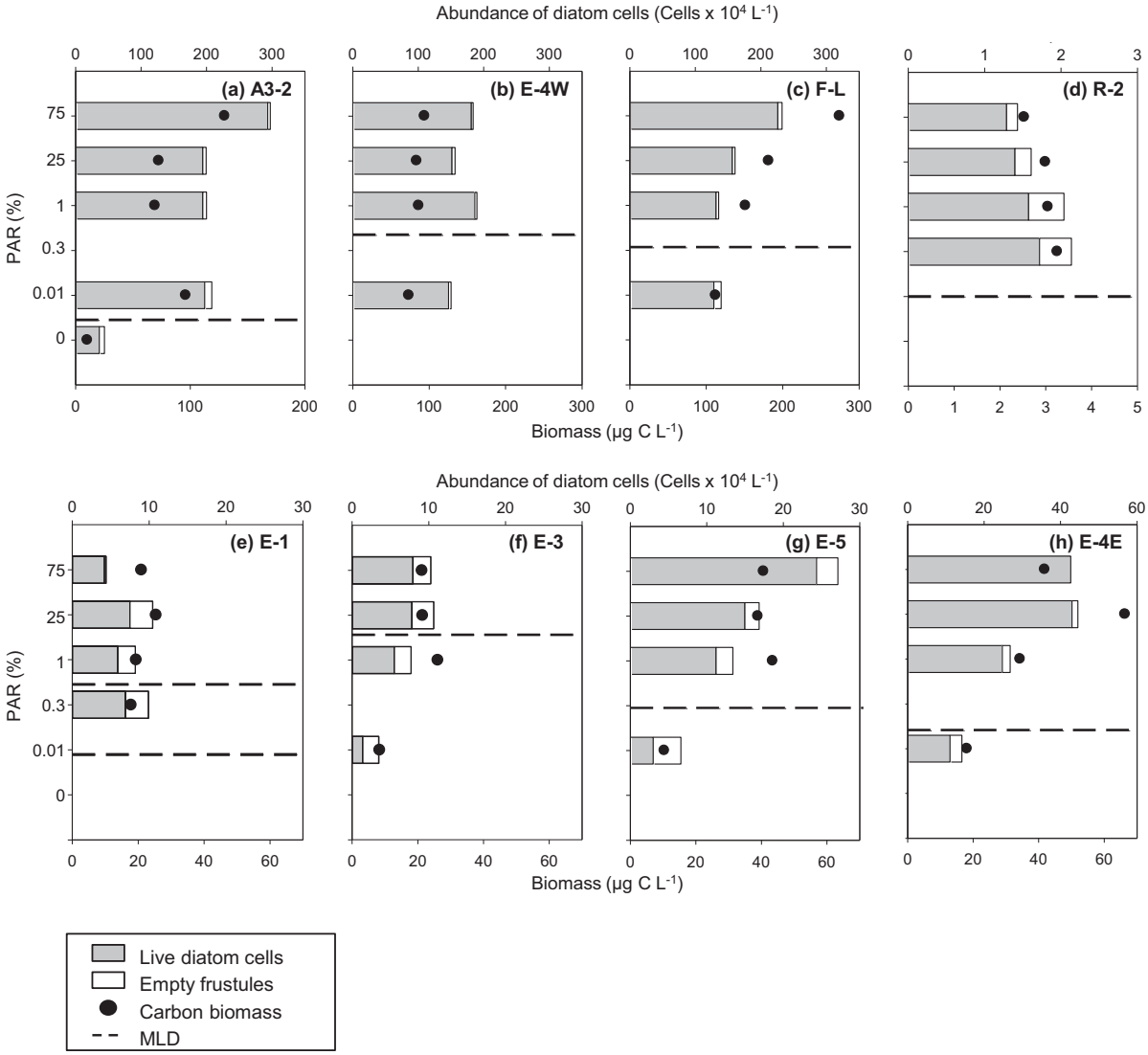

Figure 2. Vertical distributions of live cell abundance (in gray), empty frustule abundance (in white) and carbon biomass (black dots) of diatoms at each studied station. The dashed line indicates the approximate location of the mixed layer depth (MLD). A second discontinuity was identified at E-1 from the density CTD profile.

sampling provides a picture of the diatom community structure at several discrete layers over the water column, all subsequent specific diatom observations (live and empty cells) and associated C biomass estimates were based on the latter sampling methodology (detailed results are provided in Supplementary Table S2). Quantification of the proportion of diatom C biomass that was collected from net haul sampling was not undertaken in this study. Net haul results were used qualitatively to complement the vertical view of living diatom composition and community.

Specific composition of the live diatom communities

CTD rosette results from the eight studied stations indicate that the relative composition of the live diatom communities remained quite homogeneous throughout the upper water column (Fig. 4).

The two stations A3-2 and E-4W showed community similarities with an overwhelming dominance of *Chaetoceros* (*Hyalochaete*) spp. (mean 87 ± 3% of the live cells and 55 ± 6% of the C biomass), and major contributions from the small centric spp. (<25 μm; mean 5 ± 2% of the live cells and 18 ± 8% of the C biomass) and *Pseudo-nitzschia* spp. (mean 3 ± 1% of the live cells and 7 ± 3% of the C biomass).

At the station F-L, live cell abundances and C biomasses were dominated by the small centric spp. (<25 μm; respective means 54 ± 13 and 65 ± 4%) and *Chaetoceros* (*Hyalochaete*) spp. (respective means 31 ± 12 and 9 ± 5%). Station F-L was also characterized by a substantial proportion of large *Thalassiosira* spp. (>25 μm) and *Pseudo-nitzschia* spp., comprising 6 and 7%, respectively, of the total C biomass.

At all three highly productive stations, net haul results revealed major contributions of the large-sized diatoms *F. kerguelensis*, *Eucampia antarctica* and *C. pennatum* (Fig. 3). Station F-L was also characterized by an elevated live cell abundance of *Odontella weissflogii* in the upper 100 m.

At the HNLC reference station R-2, the live cell abundance was dominated by a group of pennate diatoms: *F. kerguelensis* (mean 18 ± 2%), *Fragilariopsis rhombica/separanda* (mean 8 ± 4%), *Fragilariopsis pseudonana* (mean 7 ± 4%) and *T. nitzschioides* (mean 21 ± 3%). Even though centric diatoms only represented 33% of the live cell abundance throughout the water column, they

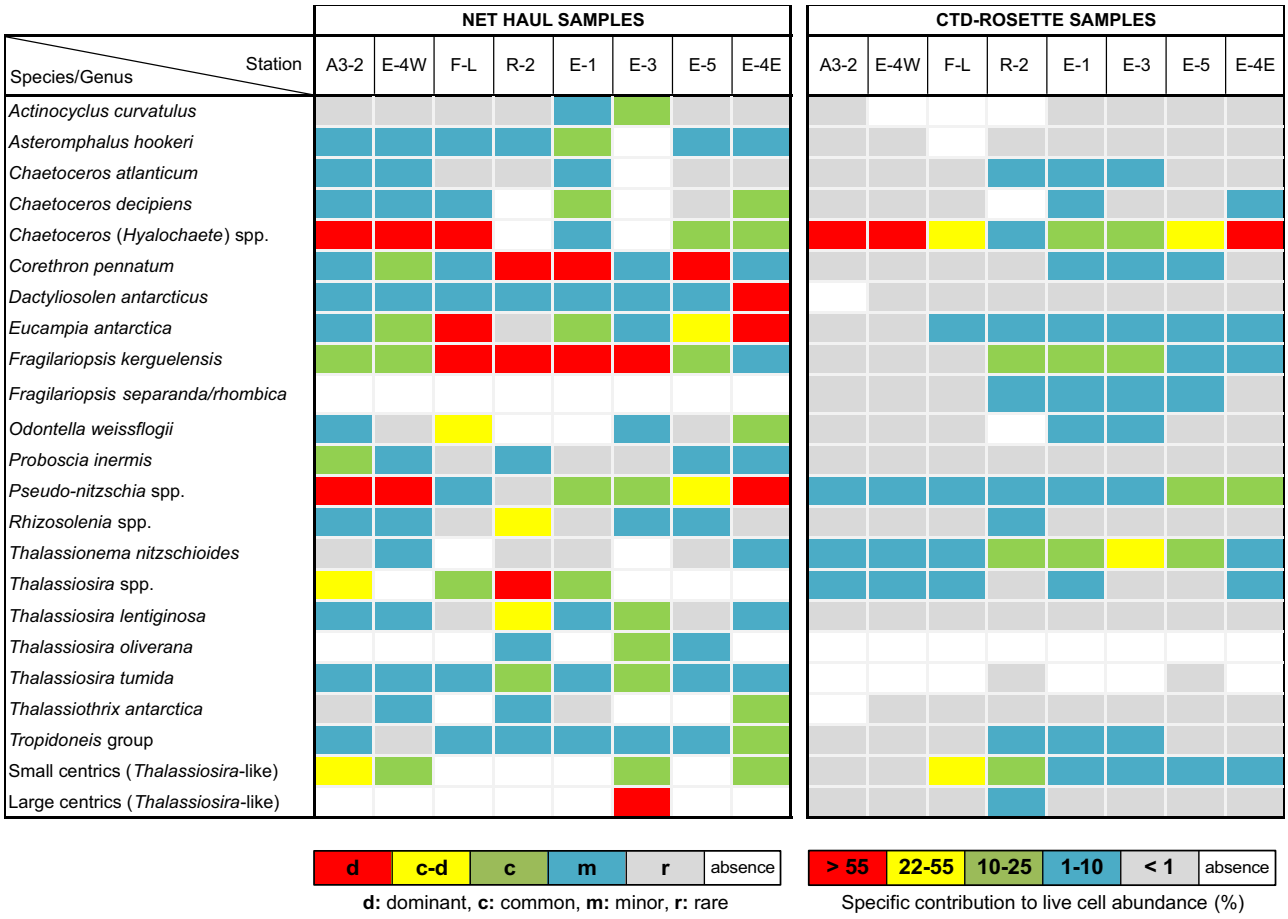

Figure 3. Qualitative assessment of diatom community composition from net hauls in the upper 100 m and comparison with the CTD rosette results averaged at all depths sampled over the water column. Only the main diatom species or genera observed over the study area are reported in this figure.

largely dominated diatom C biomass (mean 72 ± 6%). The main contributors to C biomass from 75 to 0.3% PAR were *Rhizosolenia* spp. (mean 22 ± 5%), the *Tropidoneis* group (mean 9 ± 3%), *C. pennatum* (mean 6 ± 4%) and large centric diatoms (mean 22 ± 4%) predominantly representative of *Thalassiosira* spp. (including among others *T. lentiginosa* and *T. tumida*) as net haul results suggest. Among pennate diatoms, only *F. kerguelensis* significantly contributed to the C biomass where its contribution averaged 12 ± 5% over the water column.

At the three PF meander stations sampled temporally (E-1, E-3 and E-5), the same diatom species were observed but their specific contributions to live cell abundance and C biomass changed over time (Fig. 4e–g). The first two visits (E-1 and E-3) were characterized by diatom assemblages with equally distributed species, which shifted towards a system dominated by few species (E-5). At the initial visit (E-1), the main contributors to the live cell abundance were *F. kerguelensis* (mean 18 ± 9%), *T. nitzschioides* (mean 21 ± 2%), *Chaetoceros* (*Hyalochaete*) spp. (mean 22 ± 3%) and *O. weissflogii* (mean 7 ± 2%). The temporal evolution of specific contributions to live cell abundance from the first (E-1) to the last visit (E-5) was illustrated by (i) the noticeable increase in the *Chaetoceros* (*Hyalochaete*) spp. contribution (reaching a mean of 36 ± 7%), (ii) the progressive decrease in *F. kerguelensis* and *O. weissflogii* contributions (reaching respective means of 6 ± 4 and >1%), and (iii) the constant contribution of *T. nitzschioides* (mean 17 ± 3%). Net haul results captured similar temporal evolution in the diatom community composition and highlighted the major contribution of the large diatom species *C. pennatum* and *F. kerguelensis* when compared with live cell abundance in the upper 100 m (Fig. 3). The C biomasses were dominated by *C. pennatum* over the water column (mean 42 ± 9%) at the three PF meander stations E-1, E-3 and E-5 (Fig. 4e–g). From E-1 to E-5, species-specific contributions to C biomass followed the same temporal evolution with those of the live cell abundance over the water column by showing increasing contributions of *Chaetoceros* (*Hyalochaete*) spp. (from 0.8 ± 0.1 to 10 ± 2%) and decreasing contributions of *F. kerguelensis* and *O. weissflogii* (respectively from 13 ± 6 to 3 ± 2% and from 11 ± 6 to 2 ± 1%).

CTD rosette results demonstrated that station E-4E was clearly differentiated from the other PF meander stations E-1, E-3 and E-5, as exemplified by the dominance of *Chaetoceros* (*Hyalochaete*) spp., *Pseudo-nitzschia* spp. and *Thalassiosira* spp. (<25 μm) (highest to lowest abundances; Fig. 4h). Moreover, net haul observations revealed a substantial occurrence of the large chain-forming diatoms *D. antarctica* and *E. antarctica*, and the narrow and elongated diatom *Thalassiothrix antarctica* (Fig. 3). Large diatoms such as large *Thalassiosira* spp. (>25 μm), *C. pennatum*, *E. antarctica* and species belonging to the *Tropidoneis* group (Fig. 4h) dominated the C biomass at station E-4E, even though in CTD samples these diatoms were present in lower abundances.

Chaetoceros resting spores were only found at the low light levels of 0.01% PAR at F-L, E-3 and E-5 and 0% PAR at station A3-2, contributing to <1% of the live cell abundance and total C biomass (Fig. 4).

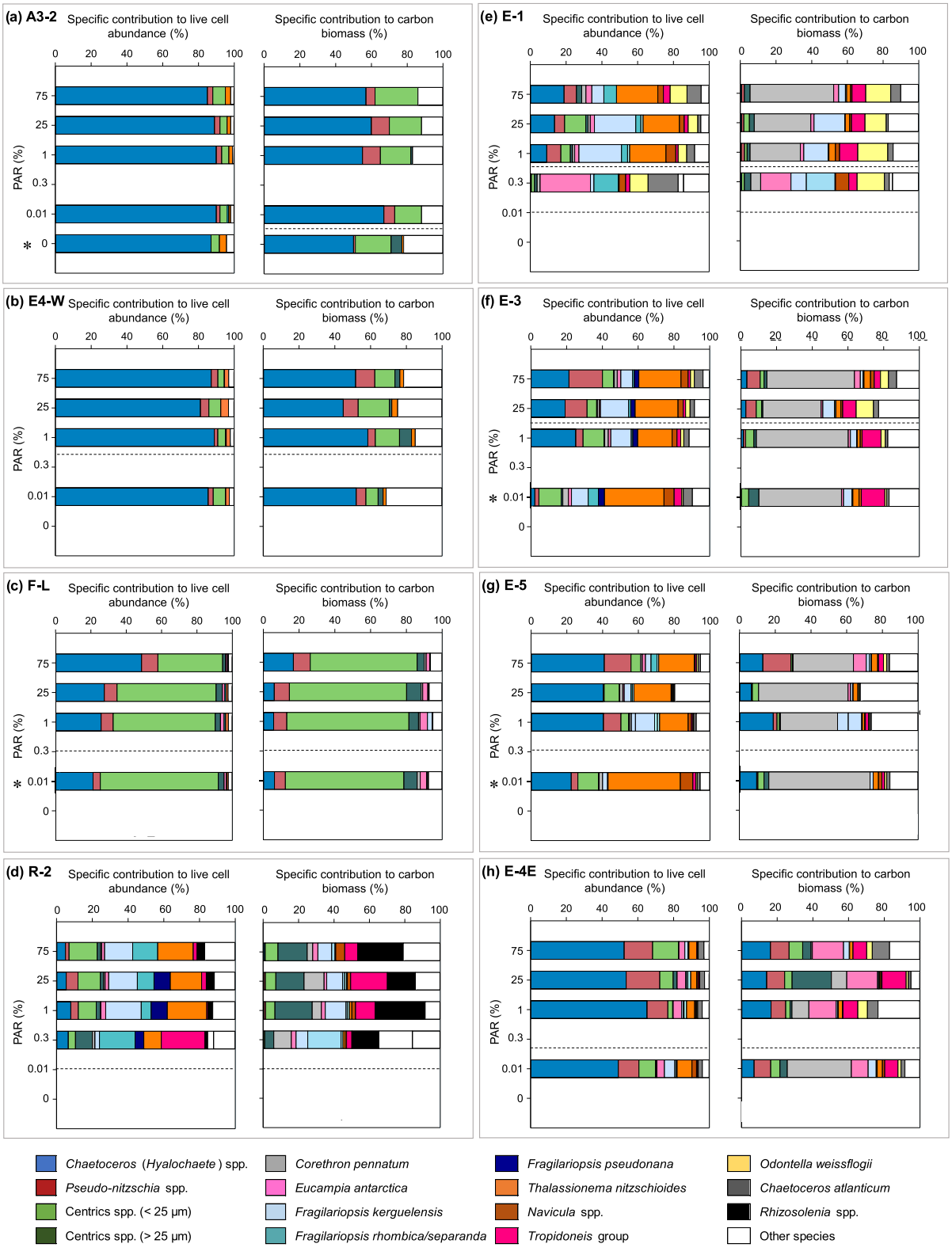

Figure 4. Vertical distributions of the relative contributions of major diatom species (as a percentage) to live cell abundance and carbon biomass at each studied station. The asterisk in front of a given light level indicates the presence of *Chaetoceros* resting spores. 'Other species' corresponds to low cell abundance and biomass species (≤1% of contribution). The dashed line indicates the approximate location of the mixed layer depth (MLD) and the second discontinuity observed at E-1.

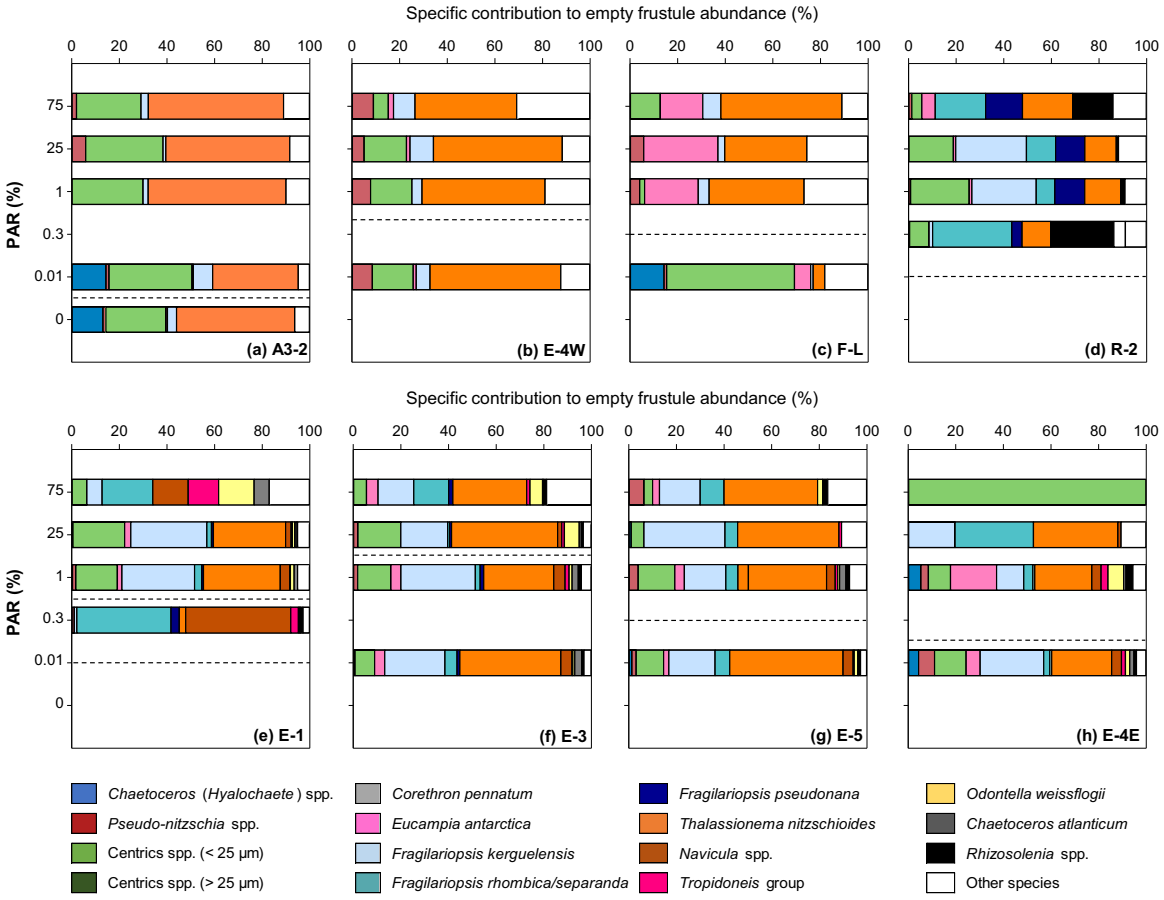

Figure 5. Vertical distributions of the relative contributions of major diatom species to empty frustule abundance (%) at each studied station. Details as in Fig. 4.

Specific contribution to empty frustule abundance

Empty frustule abundances across all three highly productive stations (A3-2, E-4W, F-L) were mainly composed by the same diatom species: *T. nitzschioides*, the small centric spp. (<25 μm), *F. kerguelensis*, *Chaetoceros* (*Hyalochaete*) spp. and *Pseudo-nitzschia* spp. (highest to lowest abundances; Fig. 5a–c). Only station F-L was characterized by a large contribution of empty *E. antarctica* (24 ± 7%) cells within the euphotic layer, whilst below the mixed layer, small centric diatoms dominated the empty cell abundance (54%). Empty frustules of *Chaetoceros* (*Hyalochaete*) spp. were only found below the euphotic layer at A3-2 (14 ± 1%) and F-L (14%).

At station R-2, empty frustules were primarily represented by *T. nitzschioides* (mean 19 ± 6%), small unidentified centric diatoms (<25 μm; mean 14 ± 9%) and three *Fragilariopsis* species through the water column. *Fragilariopsis rhombica/separanda* (11 ± 7%) and *F. pseudonana* (13 ± 2%) were major contributors to the empty frustule abundance across 75 to 0.3% PAR, whereas *F. kerguelensis*' contribution reached an average 30 ± 3% from 25 to 0.3% PAR (Fig. 5d). Elevated contributions to the empty frustule abundance were observed for *Rhizosolenia* spp. only at 75% PAR (17% in comparison with 3 ± 2% between 25 and 0.3% PAR).

At the three PF meander stations E-1, E-3 and E-5 sampled temporally, empty frustule abundances were dominated by *T. nitzschioides* (mean 31 ± 12%), *F. kerguelensis* (mean 24 ± 10%) and *Thalassiosira* spp. (<25 μm; mean 12 ± 6%) (Fig. 5e–g). Of these three stations, only E-1 exhibited a dissimilar empty frustule diatom composition at 75% PAR, with the dominance of *F. rhombica/separanda* (21%), *Navicula* spp. (15%), the *Tropidoneis* group (13%), *O. weissflogii* (15%) and *Chaetoceros atlanticum* (6%).

Station E-4E was furthermore differentiated from the three other E stations located in the meander of the PF by a distinct, heterogeneous species-specific contribution to the empty frustule abundance despite no apparent physical and biogeochemical heterogeneity (Fig. 5h). Surprisingly, at 75% PAR all the empty frustules observed corresponded to *Thalassiosira* spp. (<25 μm). From 25 to 0.01% PAR, the *Thalassiosira* spp. contribution was decreased to a tenth of the 75% PAR value (<11%) whereas *T. nitzschioides* and *F. kerguelensis* were found to be the major contributors in the underlying deep waters (29 ± 7 and 19 ± 6%, respectively). Unique elevated abundances in the empty frustules of *F. rhombica/separanda* (33%) and *E. antarctica* (20%) were observed at 25 and 1% PAR, respectively.

Contribution of functional plankton groups to total C biomass

In order to evaluate the potential contribution of diatoms to the total C biomass in the water column, the C biomass of planktonic groups (from pico- to micro-sized organisms) was estimated within the euphotic and subeuphotic layers from the eight studied stations (Fig. 6; detailed results are provided in Supplementary Table S3). Microscope observations revealed that copepod *nauplii*, acantharians, foraminifera and radiolarians were minor contributors to the total C biomass (approximatively <2%; data not shown) at each studied site.

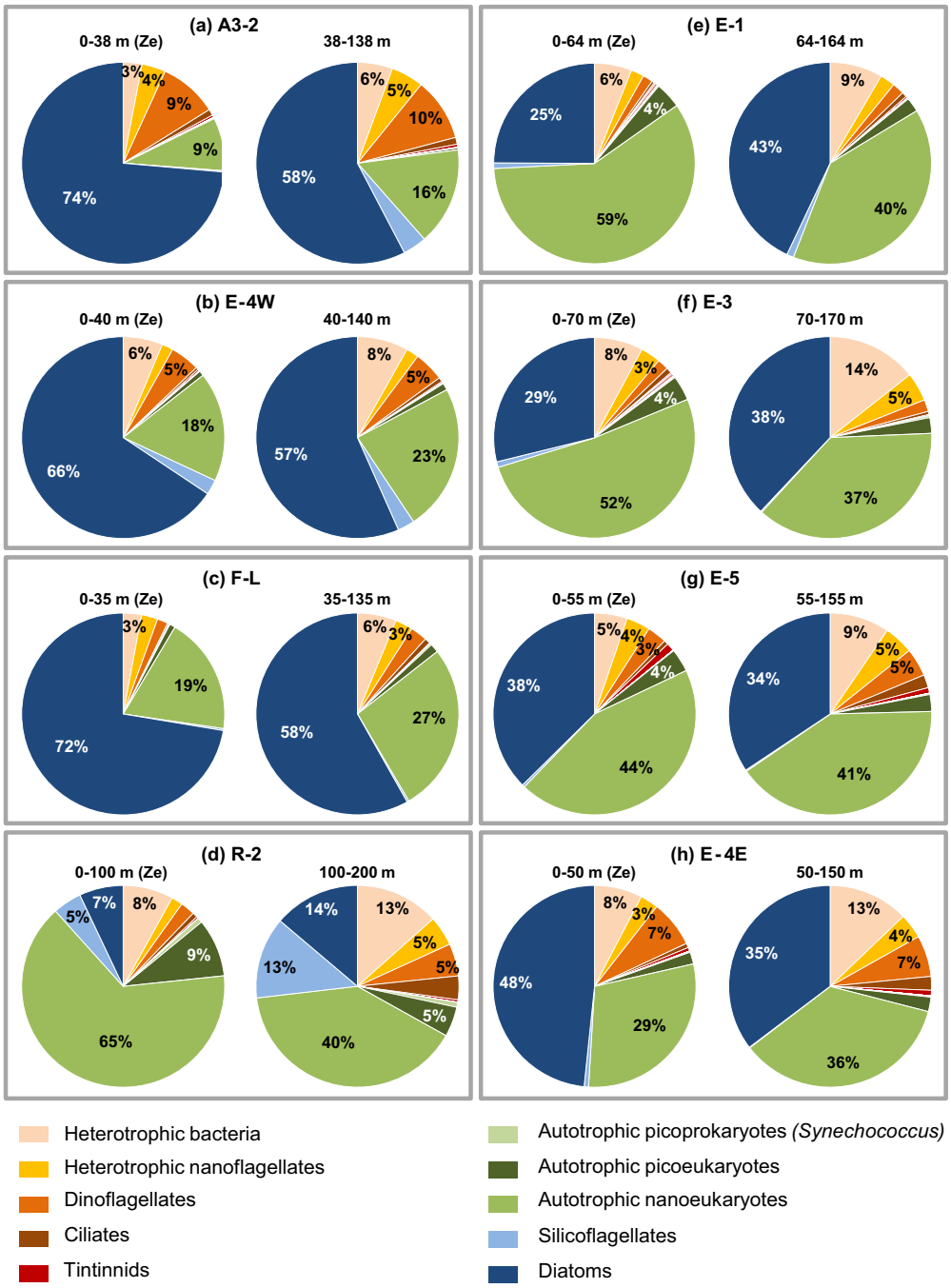

Figure 6. Relative contribution of each plankton group to carbon biomass (%) at the eight studied stations within the euphotic layer and the subeuphotic layer (defined as the layer extending 100 m below the euphotic depth, Ze). The color code ensures easy identification of autotrophic and heterotrophic organisms: blue–green colors are associated to autotrophic organisms while heterotrophic organisms are represented in red–orange.

The C biomass of autotrophs dominated the euphotic and subeuphotic layers at all stations, accounting on average for 83 ± 6% of total C biomass. Nanoeukaryotes and diatoms were the most important C contributors, but their contributions varied from one site to another. At the highly productive stations (A3-2, E-4W and F-L; Fig. 6a–c), diatoms largely dominated total C biomass in the top 200 m, representing on average 70 ± 4 and 58 ± 1% in the euphotic and subeuphotic layers, respectively. Nanoeukaryotes increased their C biomass contributions in the subeuphotic layer (mean 22 ± 6%) in comparison with the euphotic zone (mean 15 ± 6%). In the euphotic layer of the HNLC station (R-2; Fig. 6d) autotrophic nanoeukaryotes dominated the C biomass (65%). Picoeukaryotes (9%), heterotrophic bacteria (8%) and diatoms (7%) provided relatively equal proportions as the next dominant C biomass contributors in the euphotic zone. Below, in the subeuphotic layer at R-2, the autotrophic nanoeukaryote contribution decreased to 40%, while silicoflagellates, diatoms and heterotrophic bacteria

each contributed 13–14% (combined total 40%) to the total C biomass.

At the time series stations E-1, E-3 and E-5, the C biomass contributions were dominated by autotrophic nanoeukaryotes in the euphotic layer (representing 59, 52 and 44% of the total C biomass, respectively; Fig. 6e–g). However, between stations E-1 and E-5, the autotrophic nanoeukaryote contribution to the total C biomass was eroded by increasing diatom C biomass input (from 25% at E-1 to 38% at E-5). Notably, diatom contributions to C biomass were clearly higher in the subeuphotic layer (mean 41 ± 4%) than in the euphotic layer (mean 27 ± 3%) during the first two repeat station visits (E-1, E-3) and were then found to be of equivalent proportions across both layers at station E-5 (mean 36 ± 2%). At the remaining station located in the meander of the PF (E-4E), the contribution of diatoms to C biomass (48%) in the euphotic layer was clearly higher than the autotrophic nanoeukaryote contribution (29%, Fig. 6h). Station E-4E also stood out from the three other stations (E-1, E-3 and E-5) with higher C biomass contributions from dinoflagellates in both layers (7%). Finally, in the subeuphotic layer, all E stations located in the meander of the PF were characterized by higher heterotrophic community (i.e. bacteria, nanoflagellates and dinoflagellates) C biomass contributions (mean 21 ± 5%) than the values estimated from this community in the euphotic zone (mean 15 ± 4%; Fig. 6e–h; Supplementary Table S3).

DISCUSSION

Phenology of the eastern Kerguelen blooms

Early spring bloom in the northeastern Kerguelen area

In early spring, the eastern Kerguelen plateau oceanographic region was characterized by a mosaic of biogeochemical environments as reflected, for example, in the particulate matter distribution (Lasbleiz *et al.* 2014), primary production (Cavagna *et al.* 2015) and biogenic silica production (Closset *et al.* 2014). Together these observations suggest a dynamic region, host to diverse phytoplankton communities at differing stages of development, as similarly reported in other naturally iron-fertilized systems of the Southern Ocean (Pollard *et al.* 2007; Tarling *et al.* 2012).

The pseudo-Lagrangian study in the meander of the PF exemplifies the evolving bloom community in response to complex mesoscale conditions. The two first visits (E-1 and E-3) were associated with non-blooming conditions (Closset *et al.* 2014; Lasbleiz *et al.* 2014; Table 1), the dominance of nano- and picophytoplankton communities (Fig. 6), and a high proportion of empty frustules throughout the water column (Fig. 2). These non-blooming conditions were attributed to the instability of the mixed layer (Closset *et al.* 2014; Lasbleiz *et al.* 2014) as suggested by the CTD vertical density profiles (Fig. 2 in Laurenceau-Cornec *et al.* 2015). In our study, the observation of an elevated relative contribution of diatoms with respect to C biomass in the subeuphotic layer at E-1 and E-3 (Fig. 6) suggests that a short-lived diatom bloom was terminated prior to the first sampling event (E-1) as a response to adverse light-mixing conditions (Closset *et al.* 2014; Lasbleiz *et al.* 2014). Station E-1 was notably characterized by the presence of a secondary pycnocline around 130 m depth, suggestive of episodic deep-water mixing that could have rapidly transferred blooming diatom cells from the surface waters to unfavorable light conditions at depth.

In contrast, higher particulate matter concentrations and enhanced BSi production fluxes (Closset *et al.* 2014; Lasbleiz *et al.* 2014) observed during the last visit to the PF meander (E-5) were evidence of the initiation of the main spring bloom. Our results from this last visit also signal higher diatom-sourced contributions to C biomass (Fig. 6), a three-fold increase in cell abundance and a visibly decreased proportion of empty frustules (Fig. 2) in the euphotic layer compared with the pre-bloom station observations. The ability of diatoms to rapidly accumulate in the surface waters as soon as light conditions were sufficient to trigger a phytoplankton bloom (E-5) was evident from our temporal survey. Somewhat expectedly, *Chaetoceros* (*Hyalochaete*) species revealed a remarkable increase in their relative contribution to the total live cell abundance (Fig. 4e–g) in response to favorable conditions. At the highly productive stations (A3-2, E-4W and F-L; Fig. 4a–c), where a more advanced bloom stage was evidenced (Closset *et al.* 2014; Lasbleiz *et al.* 2014), *Chaetoceros* (*Hyalochaete*) spp. and small centrics (mainly *Thalassiosira* spp.), largely dominated the phytoplankton communities. Combined, these bloom state observations imply the plankton community structure in the meander of the PF was evolving from a nanoeukaryote-dominated (unstable, non-bloom condition) to diatom-dominated (stable, bloom condition) communities, primarily composed of *Chaetoceros* (*Hyalochaete*) spp. This scenario is consistent with observations at the PF meander station E-4E, located further east compared with the other E stations (Fig. 1). Here, *Chaetoceros* (*Hyalochaete*) spp. were one of the major contributors to a two-fold increased diatom cell abundance, and BSi concentrations and silica production fluxes were slightly raised (Closset *et al.* 2014; Lasbleiz *et al.* 2014). Combined, these observations suggest that station E-4E was at a slightly more advanced stage of bloom development in comparison with station E-5. Light availability has previously been shown to play an important role in controlling the phytoplankton growth and community composition in several regions of the Southern Ocean (e.g. Wright and Van den Enden 2000; Boyd *et al.* 2001; Moore *et al.* 2007). As a relevant comparison with our study, mesoscale structures were responsible for delaying the phytoplankton bloom development in the naturally iron fertilized Crozet region (Read, Pollard and Allen 2007; Venables, Pollard and Popova 2007).

The complementary use of the CTD rosette and net haul samplings has highlighted the presence of large diatoms (e.g. *C. pennatum*, *F. kerguelensis*), which were in lower abundance in Niskin bottles than in net haul samples (Fig. 3). The same observation was made from KEOPS 1 sampling, where the large and heavily silicified *F. kerguelensis* and the giant *T. antarctica* (Armand *et al.* 2008) were dominant in net-hauled community compositions but notably absent from Niskin-sampled communities. Differences between the two sampling techniques (i.e. dissimilar phytoplankton cell size sampling bias, total water volumes and integrative *versus* discrete sampling) are the obvious reasons for the divergent community observations. However, such observation differences can also imply that two distinct diatom communities were present over the Kerguelen region in spring: one that was homogeneously distributed in the mixed layer, while another (mainly composed of very large diatoms) probably occupied discrete micro-layers heterogeneously distributed in the upper 200 m (Quéguiner, Blain and Trull 2011). Such discrete-layered, large-diatom species populations are far more likely to be efficiently sampled from net hauls than Niskin samples because of the former instrument's integrated sampling ability of the top 100 m surface waters. Across the same water column, CTD rosette sampling only subsamples discrete depths unlikely to encounter such micro-scale biological variation systematically. Our observations have illustrated the importance of complementary water column sampling (CTD rosette and net haul) in providing the most realistic vertical picture of natural

diatom assemblages. Large-celled and/or long-chained species, even present in low abundances, can be major contributors to diatom C biomass, as observed for *C. pennatum* at the three PF meander stations, E-1, E-3 and E-5 (Fig. 4e–g).

Seasonal evolution of the southeastern KP bloom

The phytoplankton community of the southeastern Kerguelen Plateau (KP) bloom (station A3) was investigated in early spring (October–November 2011; KEOPS 2) and in late summer (January–February 2005; KEOPS 1). Although separated temporally, the two KEOPS programs enable a picture of the Kerguelen diatom bloom's evolution to be discerned. Species belonging to the genus *Chaetoceros* (*Hyalochaete*) play a significant role in the annual KP bloom. These small, chained diatoms (exemplified by the dominant occurrence of *C. debilis*) dominated the early spring phytoplankton bloom during KEOPS 2 and were similarly reported in high abundances during KEOPS 1 (i.e. mid-January; Armand *et al.* 2008), signifying the species' potential ability to persist continuously through summer. From mid-January to early February, the phytoplankton community evolved to an almost monospecific community of *Eucampia antarctica* v. *antarctica* in the surface waters (Armand *et al.* 2008; Mosseri *et al.* 2008). During this period, Mosseri *et al.* (2008) provided evidence for the formation of a deep silica maximum (DSM) at ~100 m that was attributed to *E. antarctica* and *Chaetoceros* resting spores (Armand *et al.* 2008).

Quéguiner (2013) described a conceptual scheme for phytoplankton seasonality in naturally iron-fertilized systems. According to this scheme, differing diatom groups (e.g. lightly silicified species *versus* grazer-resistant species) would thrive in distinct niches in the water column due to different limiting factors (e.g. light availability, nutrient limitation, grazing pressure and other mortality processes). By comparison with our observations, *Chaetoceros* (*Hyalochaete*) spp. closely correspond to Quéguiner's (2013) lightly silicified diatoms, which develop rapidly over the mixed layer in early spring once light conditions become favorable and would be sustained until summer. Meanwhile, our observations of the presence of *E. antarctica* aligns with the category of grazer-resistant diatoms, where low growth rates and heavily silicified frustules progressively developed in discrete water column layers sometimes leading to the formation of a DSM (Quéguiner 2013).

The presence of *Chaetoceros* resting spores at the end of the productive period was attributed to a survival strategy in response to the depletion of silicic acid and iron stocks in the surface waters (Armand *et al.* 2008). Laboratory experiments have commonly associated the formation of *Chaetoceros* resting spores with nutrient depletion (e.g. Kuwata, Hama and Takahashi 1993; Oku and Kamatani 1999). Nevertheless, our results revealed that *Chaetoceros* resting spores were already present in early spring below the mixed layer, despite high macronutrient and iron concentrations in the surface waters (Table 1). This implies that *Chaetoceros* resting spore formation would appear to be primarily controlled by light availability in spring at the southeastern KP station, as has been previously assumed in the North Atlantic Ocean (Rynearson *et al.* 2013). Interestingly, this observation could also support Armand *et al.* (2008)'s hypothesis that the constant presence of *Chaetoceros* resting spores below the pycnocline would allow the sustenance of a *Chaetoceros* (*Hyalochaete*) spp. bloom throughout the entire productive period. The enhanced vertical mixing characterizing the southeastern KP (Park *et al.* 2008b) thus is highly likely to facilitate the continuous seeding of *Chaetoceros* resting spores to surface waters.

Comparison with previous artificial and natural iron-fertilization experiments

Diatom community composition at station R-2 fits with typical diatom assemblages of HNLC systems as described by Smetacek, Assmy and Henjes (2004), being composed of larger and more heavily silicified species (e.g. *Rhizosolenia* spp., *Fragilariopsis* spp.), and/or species that possessed robust spines (e.g. *C. pennatum*), than species commonly found in iron-replete conditions (Kopczyńska, Fiala and Jeandel 1998; Smetacek, Assmy and Henjes 2004; Poulton *et al.* 2007). HNLC areas have also been reported as hosting a background diatom assemblage composed of lightly silicified and/or small size species (Smetacek, Assmy and Henjes 2004), such as the *Chaetoceros* (*Hyalochaete*) spp. and small centric communities, which were also encountered at R-2 (Fig. 4e). A similarly structured plankton community was observed at the KERFIX station, located further south of the station R-2 (50°40′S, 68°25′E) at the limit between the HNLC area and the western Kerguelen Plateau. At this site, diatoms only ever contributed 11% C biomass between the years 1990 to 1995. Species analyses from this study indicate that *F. kerguelensis* and *T. nitzschioides* were the principal diatom contributors with other seasonally occurring species (*Chaetoceros* spp., *Pseudo-nitzschia* spp., *F. pseudonana* and *C. pennatum*; Fiala *et al.* 1998).

The dominant species found at the highly productive iron-fertilized stations (A3-2, E-4W and F-L) belonged to the taxa groupings *Chaetoceros* (*Hyalochaete*) spp. and *Thalassiosira* spp. (Fig. 4a–c). These two taxa groups are commonly found in iron-induced blooms (Smetacek, Assmy and Henjes 2004) and their stimulation in mesoscale iron-enrichment experiments conducted in polar regions (Southern Ocean: Assmy *et al.* 2007, 2013; Boyd *et al.* 2007; Subarctic Pacific: Tsuda *et al.* 2003) has been well documented. Of particular note, artificial iron enrichment in the South Atlantic produced a *C. debilis* cell abundances 150-fold higher compared with the initial abundances (EisenEx, Assmy *et al.* 2007). The KEOPS 1 and 2 results combined suggest that a similar expansive response in cell abundances in the *Chaetoceros* (*Hyalochaete*) spp. occurs in the naturally fertilized Kerguelen region between pre-bloom spring and the end of summer (Armand *et al.* 2008).

One major difference between the naturally iron-fertilized Kerguelen blooms and the previous Southern Ocean mesoscale iron-enrichment experiments was the lower contribution of the oceanic diatoms *F. kerguelensis* and *Pseudo-nitzschia* spp. to diatom C biomass (e.g. IronEx II, Coale 1996; SOIREE, Gall *et al.* 2001) as compared with the neritic *Chaetoceros* (*Hyalochaete*) spp. This notable difference stokes the uncertainty surrounding the validity of comparing naturally iron-fertilized blooms, usually located in the vicinity of islands and possibly viewed as extensions of coastal blooms, with iron-induced blooms in the open-ocean (Smetacek and Naqvi 2008; Salter *et al.* 2012; Quéguiner 2013). In our study, the influence of the KP on the phytoplankton community composition is clear from the high contribution of the *Chaetoceros* (*Hyalochaete*) spp. to cell abundance and C biomass in the northeast Kerguelen blooms (Fig. 4). This phytoplankton response is considered to be influenced by the northward lateral advection of waters coming from the plateau across the Heard and McDonald Islands to the northeast Kerguelen region (Park *et al.* 2008a, 2014b; Lasbleiz *et al.* 2014; Bowie *et al.* 2015). In our easternmost sampled station (Station F-L) the additional effect of the northeastward drift of the coastal waters driven by the Subantarctic surface water flow (Blain *et al.* 2001; Bucciarelli, Blain and Tréguer 2001; d'Ovidio *et al.* 2015) undoubtedly modified the phytoplankton community. The hydrographic properties

of the eastern KP region have been shown to generate complex interactions between water masses with distinct origins and biogeochemical characteristics (Park *et al.* 2014b). The notable presence of typical open-ocean species in the northeastern Kerguelen blooms (e.g. *F. kerguelensis* at station F-L or *T. antarctica* and *D. antarctica* at station E-4E; Fig. 3) provides evidence of phytoplankton community compositions that are not the result of coastal bloom extensions into the Southern Ocean. The influence of the open-ocean on the northeastern Kerguelen blooms was also supported by the mesozooplankton community composition, where, for example, high abundances of oceanic species such as the copepods *Ctenocalanus citer* (typical of oceanic Subantarctic and Antarctic waters) and *Scolecithricella minor* (cosmopolitan species; Carlotti *et al.* 2015) were observed. Phytoplankton community composition of the naturally iron-fertilized Kerguelen blooms are therefore the result of complex interactions (e.g. interspecific competition, top-down control) between plankton communities originated from both coastal and open-ocean waters. Our observations would explain the noticed discrepancy with previous mesoscale iron-enrichment experiments.

Potential contribution of surface phytoplankton community structure on C export

When comparing C biomass across functional planktonic groups (Fig. 6) with concurrent biogeochemical observations, our results confirmed that diatoms largely dominated C biomasses from the surface to 200 m within the natural iron-fertilized blooms (i.e. the stabilized, final bloom conditions observed at A3-2, E-4W and F-L). These observations suggest that surface diatom communities of the iron-fertilized systems can be considered a potentially valuable vector of C export to the deep ocean. This idea is in accordance with sediment trap results from the stations A3-2 and F-L, where particle fluxes around 100 and 200 m were mainly mediated through diatom-dominated phytodetrital and fecal aggregates (Laurenceau-Cornec *et al.* 2015). Unfortunately, the composition of aggregates in the latter study was not specifically determined so the diatoms responsible for particle fluxes in the upper 200 m were not identified. However, our observations by light microscopy from CTD rosette samples suggested numerous aggregates of *Chaetoceros* (*Hyalochaete*) spp. at the A3-2 and E-4W stations, as well as abundant fecal pellets (50–100 μm) composed of small centric diatoms (<25 μm, including *Thalassiosira* spp.) at station F-L (data not shown).

Comparison with the composition of the diatom assemblage collected in a sediment trap around 290 m at A3-2 station (Rembauville *et al.* 2015) over the KP reveals a striking feature: diatom species dominating the exported material below 200 m did not correspond to the dominant *Chaetoceros* (*Hyalochaete*) spp. in the surface waters. Total diatom flux was mainly mediated by empty frustules of the small centric diatoms (<25 μm, including *Thalassiosira* spp.) and the heavily silicified diatoms *T. nitzschioides* and *F. kerguelensis* (Rembauville *et al.* 2015) that dominated empty frustule abundance in the upper 200 m (Fig. 5). This noticeable feature suggests that these heavily silicified diatoms were more efficiently exported than the lightly silicified *Chaetoceros* (*Hyalochaete*) spp. cells, likely due to the species-specific variability in their cell properties (morphology, life cycle, elemental composition, aggregate formation and potential rapid remineralization) and interactions with higher trophic levels (Assmy *et al.* 2013; Quéguiner 2013; Laurenceau-Cornec *et al.* 2015). During the CROZEX natural iron-fertilization study (Pollard *et al.* 2007), selective export of large and heavily silicified diatoms (i.e. *E. antarctica* resting spores) was similarly observed as a result of the bloom conditions north of the Crozet Plateau (Salter *et al.* 2012).

Interestingly, this feature closely aligns with two crucial biogeochemical features characterizing the KP bloom in early spring (as interpreted from station A3-2). First, the unexpected low C export efficiency reported below 200 m (Planchon *et al.* 2015) despite the high accumulation of C and BSi biomass in the surface layers (Lasbleiz *et al.* 2014) could be related to the retention of the dominant *Chaetoceros* (*Hyalochaete*) spp. cells (>55% of the C biomass) in the surface waters. Second, the KP spring bloom was assumed to behave as a silicon pump via the observation of unusually high silicon to carbon ratios in the upper 200 m (i.e. bulk particulate matter and uptake rates; Closset *et al.* 2014; Lasbleiz *et al.* 2014) and in exported material around 290 m (Rembauville *et al.* 2015). Such findings are inevitable given that empty frustules of typical heavily silicified species (*T. nitzschioides* and *F. kerguelensis*; e.g. Assmy *et al.* 2007) would be preferentially exported over the dominant *Chaetoceros* (*Hyalochaete*) spp. live cells.

All these observations combined clearly illustrate the close link between oceanic biogeochemical cycles and phytoplankton communities at the species-specific level. This emphasizes the need to go further than the diatom functional group concept and to focus on biological interactions at the individual species level in order to better understand the key factors controlling the fate of iron-induced blooms from surface waters to the seafloor (Laurenceau-Cornec *et al.* 2015; Rembauville *et al.* 2015; Rigual-Hernández *et al.* 2015a).

CONCLUSION

Spatial differences in the plankton community structures were tightly linked to the evolving stage of phytoplankton development dependent on the physical and chemical characteristics of the study areas. The iron-limited HNLC area (R-2) was typically characterized by autotrophic nanoeukaryote-dominated communities with low C biomass contributions from large and highly silicified diatom species (e.g. *Fragilariopsis* spp., *Rhizosolenia* spp., *Corethron pennatum*). Despite iron-replete stocks, comparable plankton communities were reported in the meander of the PF at the beginning of the mission (Stations E-1 and E-3) where non-blooming conditions were previously reported. The start of a well-established spring bloom in this area (Stations E-4E and E-5) was characterized by a remarkable increase in the C biomass contribution of diatoms, and especially those of *Chaetoceros* (*Hyalochaete*) spp. This genus together with an assemblage of small centric diatoms (mainly composed of *Thalassiosira* spp.) overwhelmingly dominated the well-established spring blooms at three different sites over the eastern KP area (Stations A3-2, E-4W and F-L).

Our observations confirmed that diatoms largely dominated C biomass in the naturally iron-fertilized surface waters, suggesting their potential for exporting C to the deep ocean compared with HNLC systems. Despite the high contribution of *Chaetoceros* (*Hyalochaete*) spp. to the northeastern Kerguelen blooms, the notable presence of typical open-ocean species implied that the phytoplankton community composition would be the result of complex interactions (e.g. interspecific competition, top-down control) between plankton communities originated from both coastal and open-ocean waters.

Combining the KEOPS 1 and 2 mission data sets from the southeastern KP station (station A3-2) revealed the sustained dominance of *Chaetoceros* (*Hyalochaete*) spp. throughout the

productive period (from mid-November to mid-January). We hypothesize that this sustained presence and dominance is due to the continuous seeding of *Chaetoceros* resting spores from below the pycnocline up into the surface waters. Regardless of their input and continued surface development, the dominant *Chaetoceros* (*Hyalochaete*) cells were found to be less efficiently exported than diatom species with low abundances in early spring. Such knowledge highlights the key role of species-specific cell properties and trophic interactions on matter export efficiency. Our study emphasizes the importance of exploring the specific composition of natural diatom assemblages in relation to biogeochemical parameters to better understand the functioning of marine biogeochemical cycles. We believe our results call for continued exploration of spatio-temporal scale responses appropriate to the dynamics of biological processes (e.g. silicification at the cellular scale, biological compartment interactions) while considering key environmental factors shaping phytoplankton community ecology and structure.

SUPPLEMENTARY DATA

Supplementary data are available at FEMSEC online.

ACKNOWLEDGEMENTS

We thank the KEOPS coordinator Prof. Stéphane Blain, Captain Bernard Lassiette and crew of the *R/V Marion Dufresne II* for their support aboard. We acknowledge the assistance of Véronique Cornet-Barthaux (MIO) for phytoplankton sampling. MODIS (NASA) satellite ocean-color images courtesy of Francesco d'Ovidio (UPMC, Univ. Paris), produced by Ssalto/Duacs and CLS with support from CNES. We thank the two anonymous referees for their constructive comments.

FUNDING

This work was supported by the French Research program of INSU-CNRS LEFE–CYBER (Les enveloppes fluides et l'environnement – Cycles biogéochimiques, environnement et ressources); the French ANR (Agence Nationale de la Recherche, SIMI-6 program); the French CNES (Centre National d'Études Spatiales); the French Polar Institute IPEV (Institut Polaire Paul–Emile Victor); an Endeavour Research Fellowship [grant to M.L.]; and an Australian Antarctic Division science support grant [AAS 3214 to L.A.].

Conflict of interest. None declared.

REFERENCES

Armand LK, Cornet-Barthaux V, Mosseri J *et al.* Late summer diatom biomass and community structure on and around the naturally iron-fertilised Kerguelen Plateau in the Southern Ocean. *Deep Sea Res Part II Top Stud Oceanogr* 2008;**55**: 653–76.

Armstrong RA, Peterson ML, Lee C *et al.* Settling velocity spectra and the ballast ratio hypothesis. *Deep Sea Res Part II Top Stud Oceanogr* 2009;**56**:1470–8.

Assmy P, Henjes J, Klaas C *et al.* Mechanisms determining species dominance in a phytoplankton bloom induced by the iron fertilization experiment EisenEx in the Southern Ocean. *Deep Sea Res Part I Oceanogr Res Pap* 2007;**54**:340–62.

Assmy P, Smetacek V, Montresor M *et al.* Thick-shelled, grazer-protected diatoms decouple ocean carbon and silicon cycles in the iron-limited Antarctic Circumpolar Current. *Proc Natl Acad Sci U S A* 2013;**110**:20633–8.

Blain S, Tréguer P, Belviso S *et al.* A biogeochemical study of the island mass effect in the context of the iron hypothesis: Kerguelen Islands, Southern Ocean. *Deep Sea Res Part I Oceanogr Res Pap* 2001;**48**:163–87.

Blain S, Quéguiner B, Armand L *et al.* Effect of natural iron fertilization on carbon sequestration in the Southern Ocean. *Nature* 2007;**446**:1070–4.

Bowie AR, van der Merwe P, Quéroué F *et al.* Iron budgets for three distinct biogeochemical sites around the Kerguelen Archipelago (Southern Ocean) during the natural fertilisation study, KEOPS-2. *Biogeosciences* 2015;**12**:4421–45.

Boyd PW. Diatom traits regulate Southern Ocean silica leakage. *Proc Natl Acad Sci U S A* 2013;**110**:20358–59.

Boyd PW, Crossley AC, DiTullio GR *et al.* Control of phytoplankton growth by iron supply and irradiance in the subantarctic Southern Ocean: Experimental results from the SAZ Project. *J Geophys Res Oceans* 2001;**106**:31573–83.

Boyd PW, Jickells T, Law CS *et al.* Mesoscale iron enrichment experiments 1993–2005: Synthesis and future directions. *Science* 2007;**315**:612–17.

Bucciarelli E, Blain S, Tréguer P. Iron and manganese in the wake of the Kerguelen Islands (Southern Ocean). *Mar Chem* 2001;**73**:21–36.

Buesseler KO, Andrews JE, Pike SM *et al.* Particle export during the Southern Ocean iron experiment (SOFeX). *Limnol Oceanogr* 2005;**50**:311–27.

Buesseler KO, Boyd PW. Shedding light on processes that control particle export and flux attenuation in the twilight zone of the open ocean. *Limnol Oceanogr* 2009;**54**:1210–32.

Carlotti F, Jouandet MP, Nowaczyk A *et al.* Mesozooplankton structure and functioning during the onset of the Kerguelen phytoplankton bloom during the KEOPS2 survey. *Biogeosciences* 2015;**12**:4543–63.

Carlotti F, Thibault-Botha D, Nowaczyk A *et al.* Zooplankton community structure, biomass and role in carbon fluxes during the second half of a phytoplankton bloom in the eastern sector of the Kerguelen Shelf (January-February 2005). *Deep Sea Res Part II Top Stud Oceanogr* 2008;**55**:720–33.

Caron DA, Dam HG, Kremer P *et al.* The contribution of microorganisms to particulate carbon and nitrogen in surface waters of the Sargasso Sea near Bermuda. *Deep Sea Res Part I Oceanogr Res Pap* 1995;**42**:943–72.

Casey JR, Aucan JP, Goldberg SR *et al.* Changes in partitioning of carbon amongst photosythethic pico- and nano-plankton groups in the Sargasso Sea in response to changes in the North Atlantic Oscillation. *Deep Sea Res Part II Top Stud Oceanogr* 2013;**93**:58–70.

Cavagna AJ, Fripiat F, Elskens M *et al.* Production regime and associated N cycling in the vicinity of Kerguelen Island, Southern Ocean. *Biogeosciences* 2015;**12**:6515–28.

Christaki U, Courties C, Massana R *et al.* Optimized routine flow cytometric enumeration of heterotrophic flagellates using SYBR Green I. *Limnol Oceanogr Methods* 2011;**9**: 329–39.

Christaki U, Georges C, Genitsaris S *et al.* Microzooplankton community associated with phytoplankton blooms in the naturally iron-fertilized Kerguelen area (Southern Ocean). *FEMS Microbiol Ecol* 2015;**91**: fiv068.

Christaki U, Lefèvre D, Georges C *et al.* Microbial food web dynamics during spring phytoplankton blooms in the naturally iron-fertilized Kerguelen area (Southern Ocean). *Biogeosciences* 2014;**11**:6739–53.

Christaki U, Obernosterer I, Van Wambeke F *et al.* Microbial food web structure in a naturally iron-fertilized area in the Southern Ocean (Kerguelen Plateau). *Deep Sea Res Part II Top Stud Oceanogr* 2008;**55**:706–19.

Closset I, Lasbleiz M, Leblanc K *et al.* Seasonal evolution of net and regenerated silica production around a natural Fe-fertilized area in the Southern Ocean estimated with Si isotopic approaches. *Biogeosciences* 2014;**11**:5827–46.

Coale KH. A massive phytoplankton bloom induced by an ecosystem-scale iron fertilization experiment in the equatorial Pacific Ocean. *Nature* 1996;**383**:495–501.

Cornet-Barthaux V, Armand L, Quéguiner B. Biovolume and biomass estimates of key diatoms in the Southern Ocean. *Aquat Microb Ecol* 2007;**48**:295–308.

de Baar H, Boyd P, Coale K *et al.* Synthesis of iron fertilization experiments: From the Iron Age in the Age of Enlightenment. *J Geophys Res* 2005;**110**:C09S16.

d'Ovidio F, Della Penna A, Trull TW *et al.* The biogeochemical structuring role of horizontal stirring: Lagrangian perspectives on iron delivery downstream of the Kerguelen Plateau. *Biogeosciences* 2015;**12**:5567–81.

Fiala M, Kopczynska EE, Jeandel C *et al.* Seasonal and interannual variability of size-fractionated phytoplankton biomass and community structure at station Kerfix, off the Kerguelen Islands, Antarctica. *J Plankton Res* 1998;**20**:1341–56.

Fukuda R, Ogawa H, Nagata E *et al.* Direct determination of carbon and nitrogen contents of natural bacterial assemblages in marine environments. *Appl Environ Microbiol* 1998;**64**:3352–58.

Gall MP, Boyd PW, Hall J *et al.* Phytoplankton processes. Part 1: Community structure during the Southern Ocean Iron RElease Experiment (SOIREE). *Deep Sea Res Part II Top Stud Oceanogr* 2001;**48**:2551–70.

Hasle GR. Using the inverted microscope. In: Sournia A (ed.). *Phytoplankton Manual*. Paris: UNESCO, 1978, 191–6.

Hasle GR, Syvertsen EE. Marine diatoms. In: Tomas CR (ed.). *Identifying Marine Phytoplankton*. San Diego: Academic Press, 1997, 5–385.

Hillebrand H, Dürselen CD, Kirschtel D *et al.* Biovolume calculation for pelagic and benthic microalgae. *J Phycol* 1999;**35**: 403–24.

Kopczyńska EE, Fiala M, Jeandel C. Annual and interannual variability in phytoplankton at a permanent station off Kerguelen Islands, Southern Ocean. *Polar Biol* 1998;**20**:342–51.

Kuwata A, Hama T, Takahashi M. Ecophysiological characterization of two life-forms, resting spores and resting cells of a marine planktonic diatom, *Chaetoceros pseudocurvisetus* formed under nutrient depletion. *Mar Ecol Prog Ser* 1993;**102**:245–55.

Landa M, Blain S, Christaki U *et al.* Shifts in bacterial community composition associated with increased carbon cycling in a mosaic of phytoplankton blooms. *ISME J* 2016;**10**:39–50.

Lasbleiz M, Leblanc K, Blain S *et al.* Pigments, elemental composition (C, N, P, and Si), and stoichiometry of particulate matter in the naturally iron fertilized region of Kerguelen in the Southern Ocean. *Biogeosciences* 2014;**11**:5931–55.

Laurenceau-Cornec EC, Trull TW, Davies DM *et al.* The relative importance of phytoplankton aggregates and zooplankton fecal pellets to carbon export: insights from free-drifting sediment trap deployments in naturally iron-fertilised waters near the Kerguelen Plateau. *Biogeosciences* 2015;**12**:1007–27.

Leblanc K, Arìstegui J, Armand L *et al.* A global diatom database – abundance, biovolume and biomass in the world ocean. *Earth Syst Sci Data* 2012;**4**:149–65.

Legendre L, Le Fèvre J. Hydrodynamical singularities as controls of recycled versus export production in oceans. In: Berger WH, Smetacek VS, Wefer G (eds). *Productivity of the Ocean: Present and Past*. Chichester: Wiley, 1989, 49–63.

Marie D, Partensky F, Vaulot D *et al.* Enumeration of phytoplankton, bacteria and viruses in marine samples. In: Robinson JP (ed.). *Current Protocols in Cytometry*. New York: John Wiley and Sons, 1999, 1–15.

Menden-Deuer S, Lessard EJ. Carbon to volume relationships for dinoflagellates, diatoms, and other protist plankton. *Limnol Oceanogr* 2000;**45**:569–79.

Moore CM, Seeyave S, Hickman AE *et al.* Iron-light interactions during the CROZet natural iron bloom and EXport experiment (CROZEX) I: Phytoplankton growth and photophysiology. *Deep Sea Res Part II Top Stud Oceanogr* 2007;**54**:2045–65.

Mosseri J, Quéguiner B, Armand L *et al.* Impact of iron on silicon utilization by diatoms in the Southern Ocean: A case study of Si/N cycle decoupling in a naturally iron-enriched area. *Deep Sea Res Part II Top Stud Oceanogr* 2008;**55**:801–19.

Nelson DM, Anderson RF, Barber RT *et al.* Vertical budgets for organic carbon and biogenic silica in the Pacific sector of the Southern Ocean, 1996–1998. *Deep Sea Res Part II Top Stud Oceanogr* 2002;**49**:1645–74.

Oku O, Kamatani A. Resting spore formation of the marine planktonic diatom *Chaetoceros anastomosans* induced by high salinity and nitrogen depletion. *Mar Biol* 1999;**127**:515–20.

Olenina I, Hajdu S, Edler L *et al. Biovolumes and Size-Classes of Phytoplankton in the Baltic Sea*. Baltic Sea Environment Proceedings No. 106. Helsinki: Helsinki Commission, Baltic Marine Environment Protection Commission, 2006.

Park Y-H, Durand I, Kestenare E *et al.* Polar Front around the Kerguelen Islands: An up-to-date determination and associated circulation of surface/subsurface waters. *J Geophys Res Oceans* 2014b;**119**:6575–92.

Park Y-H, Fuda J-L, Durand I *et al.* Internal tides and vertical mixing over the Kerguelen Plateau. *Deep Sea Res Part II Top Stud Oceanogr* 2008b;**55**:582–93.

Park YH, Lee JH, Durand I *et al.* Validation of Thorpe-scale-derived vertical diffusivities against microstructure measurements in the Kerguelen region. *Biogeosciences* 2014a;**11**:6927–37.

Park Y-H, Roquet F, Durand I *et al.* Large-scale circulation over and around the Northern Kerguelen Plateau. *Deep Sea Res Part II Top Stud Oceanogr* 2008a;**55**:566–81.

Planchon F, Ballas D, Cavagna AJ *et al.* Carbon export in the naturally iron-fertilized Kerguelen area of the Southern Ocean based on the ^{234}Th approach. *Biogeosciences* 2015;**12**:3831–48.

Pollard R, Sanders R, Lucas M *et al.* The Crozet Natural Iron Bloom and Export Experiment (CROZEX). *Deep Sea Res Part II Top Stud Oceanogr* 2007;**54**:1905–14.

Poulton AJ, Moore CM, Seeyave S *et al.* Phytoplankton community composition around the Crozet Plateau, with emphasis on diatoms and Phaeocystis. *Deep Sea Res Part II Top Stud Oceanogr* 2007;**54**:2085–105.

Putt M, Stoecker DK. An experimentally determined carbon:volume ratio for marine 'oligotrichous' ciliates from estuarine and coastal waters. *Limnol Oceanogr* 1989;**34**:1097–103.

Quéguiner B. Iron fertilization and the structure of planktonic communities in high nutrient regions of the Southern Ocean. *Deep Sea Res Part II Top Stud Oceanogr* 2013;**90**:43–54.

Quéguiner B, Blain S, Trull T. High primary production and vertical export of carbon over the Kerguelen Plateau as a consequence of natural iron fertilization in a high-nutrient,

low-chlorophyll environment. In: Duhamer G, Welsford D (eds). *The Kerguelen Plateau: Marine Ecosystem and Fisheries*. Paris: Societe Francaise d'Ichtyologie, 2011.

Quéroué F, Sarthou G, Planquette HF *et al*. High variability in dissolved iron concentrations in the vicinity of the Kerguelen Islands (Southern Ocean). *Biogeosciences* 2015;**12**:3869–83.

Read JF, Pollard RT, Allen JT. Sub-mesoscale structure and the development of an eddy in the Subantarctic Front north of the Crozet Islands. *Deep Sea Res Part II Top Stud Oceanogr* 2007;**54**:1930–48.

Rembauville M, Blain S, Armand L *et al*. Export fluxes in a naturally iron-fertilized area of the Southern Ocean – Part 2: Importance of diatom resting spores and faecal pellets for export. *Biogeosciences* 2015;**12**:3171–95.

Rigual-Hernández AS, Trull TW, Bray SG *et al*. Seasonal dynamics in diatom and particulate export fluxes to the deep sea in the Australian sector of the southern Antarctic Zone. *J Mar Syst* 2015a;**142**:62–74.

Rigual-Hernández AS, Trull TW, Bray SG *et al*. Latitudinal and temporal distributions of diatom populations in the pelagic waters of the Subantarctic and Polar Frontal zones of the Southern Ocean and their role in the biological pump. *Biogeosciences* 2015b;**12**:5309–37.

Romero OE, Armand LK. Marine diatoms as indicators of modern changes in oceanographic conditions. In: Smol JP, Stoermer EF (eds). *The Diatoms: Applications for the Environmental and Earth Sciences*. Cambridge: Cambridge University Press, 2010, 373–400.

Rynearson TA, Richardson K, Lampitt RS *et al*. Major contribution of diatom resting spores to vertical flux in the sub-polar North Atlantic. *Deep Sea Res Part I Oceanogr Res Pap* 2013;**82**:60–71.

Sackett O, Armand L, Beardall J *et al*. Taxon-specific responses of Southern Ocean diatoms to Fe enrichment revealed by synchrotron radiation FTIR microspectroscopy. *Biogeosciences* 2014;**11**:5795–808.

Salter I, Kemp AES, Moore CM *et al*. Diatom resting spore ecology drives enhanced carbon export from a naturally iron-fertilized bloom in the Southern Ocean. *Global Biogeochem Cycles* 2012;**26**:GB1014.

Smayda TJ. *From Phytoplankton to Biomass*. Paris: UNESCO, 1978.

Smetacek V, Assmy P, Henjes J. The role of grazing in structuring Southern Ocean pelagic ecosystems and biogeochemical cycles. *Antarct Sci* 2004;**16**:541–58.

Smetacek V, Klaas C, Strass VH *et al*. Deep carbon export from a Southern Ocean iron-fertilized diatom bloom. *Nature* 2012;**487**:313–19.

Smetacek V, Naqvi SWA. The next generation of iron fertilization experiments in the Southern Ocean. *Philos Trans A Math Phys Eng Sci* 2008;**366**:3947–67.

Sun J, Liu DY. Geometric models for calculating cell biovolume and surface area for phytoplankton. *J Plankton Res* 2003;**25**:1331–46.

Tarling GA, Ward P, Atkinson A *et al*. DISCOVERY 2010: Spatial and temporal variability in a dynamic polar ecosystem. *Deep Sea Res Part II Top Stud Oceanogr* 2012;**59-60**:1–13.

Tsuda A, Takeda S, Saito H *et al*. A mesoscale iron enrichment in the Western Subarctic Pacific induces a large centric diatom bloom. *Science* 2003;**300**:958–61.

Veldhuis MJW, Kraay G. Application of flow cytometry in marine phytoplankton research: current applications and future perspectives. *Sci Mar* 2000;**64**:121–34.

Venables HJ, Pollard RT, Popova EE. Physical conditions controlling the development of a regular phytoplankton bloom north of the Crozet Plateau, Southern Ocean. *Deep Sea Res Part II Top Stud Oceanogr* 2007;**54**:1949–65.

Verity P, Robertson CY, Tronzo CR *et al*. Relationships between cell volume and the carbon and nitrogen content of marine photosynthetic nanoplankton. *Limnol Oceanogr* 1992;**37**:1434–46.

West NJ, Obernosterer I, Zemb O *et al*. Major differences of bacterial diversity and activity inside and outside of a natural iron-fertilized phytoplankton bloom in the Southern Ocean. *Environ Microbiol* 2008;**10**:738–56.

Wright SW, van den Enden RL. Phytoplankton community structure and stocks in the East Antarctic marginal ice zone (BROKE survey, January–March 1996) determined by CHEMTAX analysis of HPLC pigment signatures. *Deep Sea Res Part II Top Stud Oceanogr* 2000;**47**:2363–400.